J Therm Anal Calorim (2011) 105:961–968
DOI 10.1007/s10973-011-1486-9

Synthesize, crystal structure, heat capacities and thermodynamic properties of a potential enantioselective catalyst

Ju-Lan Zeng · Sai-Bo Yu · Zhong Cao · Dao-Wu Yang · Li-Xian Sun · Ling Zhang · Xiong-Fei Zhang

Received: 15 March 2010 / Accepted: 14 December 2010 / Published online: 8 April 2011

Abstract A new potential enantioselective catalyst derived from ferrocene, 1-{(*R*)-1-[(*S*)-2-(diphenylphosphino)ferrocenyl]ethyl}-benzimidazole (DPFEB), was prepared and its absolute structure was characterized by means of single crystal X-ray diffraction. The molar heat capacity of DPFEB was measured by means of temperature modulated differential scanning calorimetry over the temperature range of 200–530 K, and the thermodynamic functions of $[H_T - H_{298.15}]$ and $[S_T - S_{298.15}]$ were calculated. Further more, thermogravimetry experiment revealed that DPFEB exhibited a three step thermal decomposition process with the final residual of 28.7%.

Keywords Enantioselective catalyst · Crystal structure · Molar heat capacity · Thermodynamic functions

Introduction

Ferrocene-based derivatives have been widely used in a lot of fields, such as electrochemistry [1–3], material science [4–6], and particularly enantioselective catalysis [7–9], because of their stability, easy introduction of planar chirality, and special electronic- and stereo-properties of the ferrocene skeleton. Recently, PPFA (shown in Scheme 1), a ferrocene-based chiral phosphorus intermediate, has been widely applied in the designing and synthesizing of chiral ligands due to its diversity in ligand preparation [10, 11]. Very recently, *N*-heterocycles contained ferrocene-based chiral phosphorus ligands, which can be synthesized from PPFA [12], have exhibited excellent enantioselectivities and catalytic activities in enantioselective catalysis [13]. In order to synthesize a series of ferrocene-based chiral phosphorus ligands containing *N*-heterocycles, we prepared 1-{(*R*)-1-[(*S*)-2-(diphenylphosphino)ferrocenyl]ethyl}-benzimidazole (DPFEB). DPFEB can be prepared from PPFA through Scheme 2. There are P and N coordinating atoms contained in DPFEB, making it have potential application in enantioselective catalysis. Further more, functional groups containing coordinating atoms such as P, S, O, and N could be introduced to the benzimidazole ring of DPFEB, making it versatile in further ligands preparation.

It is generally accepted that thermodynamic properties are one of the most critical properties of substance. The preparation and application of a substance are greatly affected by its thermodynamic properties. Heat capacity is the most fundamental thermodynamic property, from which other thermodynamic properties such as enthalpy and entropy can be obtained. However, the thermodynamics of compounds derived from ferrocene have been scarcely reported [14]. Temperature-modulated differential scanning calorimetry (TMDSC) is an easier and accurate method for determining

Ju-Lan Zeng and Sai-Bo Yu contributed equally to this study.

J.-L. Zeng (✉) · Z. Cao · D.-W. Yang · L. Zhang · X.-F. Zhang
Hunan Provincial Key Laboratory of Materials Protection for Electric Power and Transportation, School of Chemistry and Biological Engineering, Changsha University of Science and Technology, Changsha 410004, People's Republic of China
e-mail: julan_zeng@yahoo.com.cn

S.-B. Yu (✉)
China Tobacco Hunan Industrial Corporation, Changsha 410007, People's Republic of China
e-mail: saipi@163.com

L.-X. Sun
Materials and Thermochemistry Laboratory, Dalian Institute of Chemical Physics, Chinese Academy of Sciences, Dalian 116023, People's Republic of China

Scheme 1 Preparation of (R_c, S_p)-PPFA

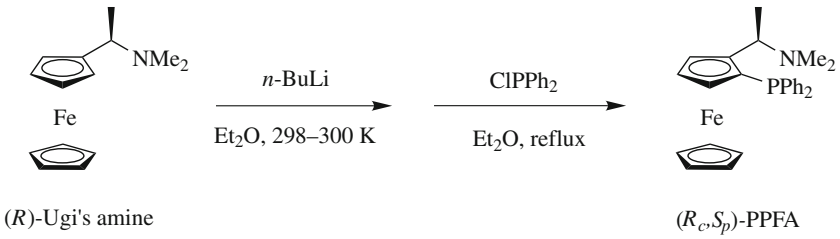

Scheme 2 Preparation of DPFEB

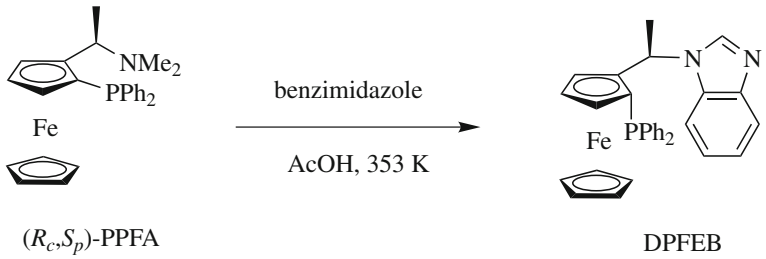

the heat capacity. The structure and principle of the calorimeter have been described in details [15, 16]. Recently, it has been greatly developed for directly determining heat capacities for various materials successfully [17–20].

In this article, the preparation and the crystal structure of DPFEB were reported. In addition, the molar heat capacities of DPFEB were measured by TMDSC and the thermodynamic parameters such as entropy and enthalpy were also calculated. The accuracy of TMDSC was established by comparing the measured heat capacities of standard sapphire (α-Al_2O_3) with previously reported values (NIST and NBS) [21, 22]. Furthermore, the thermal decomposition characteristics of this compound were also investigated.

Experimental

Sample preparation

General considerations

All reactions were carried out under nitrogen atmosphere in oven-dried glassware. Unless otherwise noted, commercial reagents were used as received without further purification. Diethyl ether (Et_2O) was distilled from sodium/benzophenone ketyl under nitrogen atmosphere. (*R*)-Ugi's amine was prepared according to a reported procedure [23].

Preparation of (R_c, S_p)-PPFA

As described in Scheme 1 [24], to a solution of (*R*)-Ugi's amine (7.2 g, 28 mmol) in Et_2O (40 mL) was added dropwise *n*-BuLi (12 mL, 30 mmol, 2.5 M solution in hexane) at 298–300 K. The reaction mixture was stirred for another 1.5 h at room temperature. The mixture was then heated to reflux, followed by dropwise addition of chlorodiphenylphosphine (12.4 g, 56 mmol) dissolved in Et_2O (20 mL). The mixture was refluxed for 4 h. The reaction was cooled in ice-water bath and quenched with saturated $NaHCO_3$ solution (~40 mL). The organic layer was separated and the aqueous layer was extracted with Et_2O. The combined organic layers were washed with water and dried over anhydrous Na_2SO_4. The solution was filtered and evaporated under reduced pressure. The residue was purified by flash column chromatography to afford (R_c, S_p)-PPFA 6.9 g. Yield: 56%, orange crystal.

Preparation of DPFEB

The preparation of DPFEB is shown in Scheme 2 [25]. A mixture of (R_c, S_p)-PPFA (4.41 g, 10 mmol) and benzimidazole (5.8 g, 50 mmol) in 50 mL degassed glacial AcOH was stirred at 353 K for 8 h. The reaction mixture was quenched with an excess saturated $NaHCO_3$ solution and extracted with CH_2Cl_2 (50 mL × 3). The combined organic extracts were washed with brine and dried over anhydrous Na_2SO_4, filtered, and evaporated under reduced pressure. The crude product was purified by flash column chromatography and then recrystallized from *n*-hexane/CH_2Cl_2 solution to afford DPFEB. Yield: 93%, orange crystal. The crystal products were grinded and dried in vacuum at 323 K for 24 h before TMDSC and TG experiments were performed.

X-ray crystallography

Suitable crystals of DPFEB were obtained by re-crystallizing it from *n*-hexane/CH_2Cl_2 solution. The diffraction data were measured on a Bruker Smart APEXII CCD area-detector diffractometer with Mo Kα radiation (λ =

Table 1 Crystal data and structure refinement parameters for DPFEB

Empirical formula	$C_{31}H_{28}FeN_2P$
Formula weight	515.37
Crystal system	Orthorhombic
Space group	P2(1)2(1)2(1)
a/Å	11.457(3)
b/Å	14.637(4)
c/Å	15.338(4)
V/Å^{-3}	2572.2(12)
Z	4
Dc/Mg m^{-3}	1.331
F (000)	1076
Absorption coefficient/mm^{-1}	0.671
Limiting indices	$-5 \le h \le 14$, $-17 \le k \le 19$, $-20 \le l \le 19$
Goodness-of-fit on F^2	1.020
R_{int}	0.049
R_1, wR_2 ($I > 2\sigma$ (I))	0.0321, 0.0668
R_1, wR_2 (all data)	0.0582, 0.0716
Largest diff. peak and hole/e Å^{-3}	0.207 and −0.256

Table 2 Selected bond lengths (Å) for DPFEB

Fe1–C1	2.034(3)	Fe1–C8	2.031(2)	C1–C5	1.398(4)
Fe1–C2	2.033(2)	Fe1–C9	2.0453(19)	C6–C7	1.404(3)
Fe1–C3	2.039(2)	Fe1–C10	2.047(2)	C7–C8	1.428(3)
Fe1–C4	2.045(3)	C1–C2	1.406(4)	C8–C9	1.448(3)
Fe1–C5	2.050(3)	C2–C3	1.410(4)	C9–C10	1.428(3)
Fe1–C6	2.051(2)	C3–C4	1.394(4)	C6–C10	1.423(3)
Fe1–C7	2.042(2)	C4–C5	1.401(4)		

0.71073 Å) using ω and φ scan mode within the range of $2.22 < \theta < 24.23$ at 273(2) K. The crystal size was 0.52 × 0.46 × 0.38 mm. Of 5804 measured reflections, 4578 observed reflections with $I > 2\sigma$ (I) were used in the refinement. The structure was solved by direct methods using SHELXS program of the SHELXL-97 package and refined with full-matrix least-squares refinements based on F^2 using SHELXL [26]. All non-H atoms were located using subsequent Fourier-difference methods and all the hydrogen atoms were placed in the geometrically calculated positions in the riding model. Crystallographic data and refinement parameters of the crystal are summarized in Table 1. Selected bond distances are given in Table 2.

Heat capacity measurement

Heat capacity measurements were carried out on a DSC Q1000 (T-zero DSC-technology, TA Instruments Inc., USA). A mechanical cooling system was used for the experimental measurement. Dry high purity (99.999%) nitrogen gas was applied as purge gas (50 mL min^{-1}). The instrument was initially calibrated in the standard DSC mode, using the extrapolated onset temperatures of the melting of indium (429.75 K) at a heating rate of 10 K min^{-1} and the heat of fusion of indium (28.45 J g^{-1}). The heat capacity calibration was made by running a standard sapphire (α-Al_2O_3) measurement at the experimental temperature. The calibration method and the experiment were performed at the same conditions as follows: (1) sampling interval: 1.00 s/pt; (2) zero heat flow at 253.15 K; (3) equilibrate at 193.15 K; (4) modulate temperature amplitude of ±0.5 K with period of 100 s; (5) isothermal for 5.00 min; and (6) temperature ramp at 10 K min^{-1} to 530 K. The constants of heat capacity for the TMDSC: $K_{total} = 1.024$; $K_{reversible} = 1.019$. The masses of the reference and sample pans with lids were measured to be 48 ± 0.02 mg. Samples were crimped in non-hermetic aluminum pans with lids. Sample mass was weighed on a METTLER TOLEDO electrobalance (AB135-S, Classic) with an accuracy of (±0.01 mg) and different samples were used in each measurement.

Thermal analysis

Thermogravimetric analysis (TG) was carried out on Cahn Thermax 500 from 300 to 1173 K. The heating rate was 10 K min^{-1} and the flow rate of N_2 was 100 mL min^{-1}. The sample mass of DPFEB was 97.33 mg. The TG equipment was calibrated by $CaC_2O_4 \cdot H_2O$ (99.9%).

Results and discussions

Crystal structure

The molecule structure of DPFEB is depicted in Fig. 1. It can be seen from Table 2 that the C–C bond lengths of

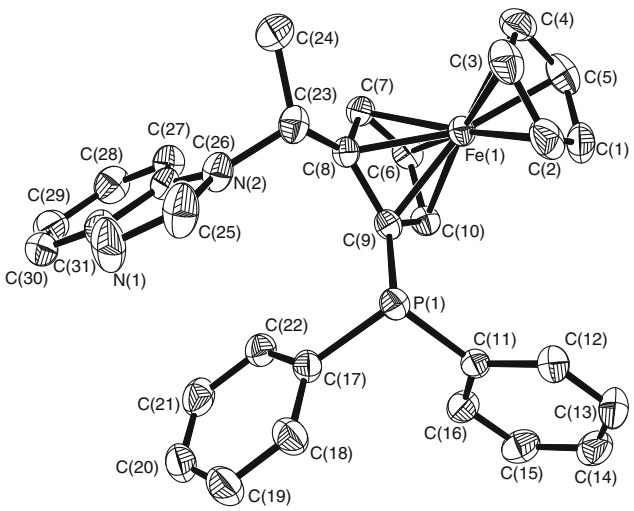

Fig. 1 The molecule structure of DPFEB

unsubstituted cyclopentadienyl ring are in the range of 1.394–1.410 Å while that of substituted cyclopentadienyl ring are in the range of 1.404–1.448 Å. The C–C bonds of substituted cyclopentadienyl ring become longer due to the effect of the substituent. The bond length of C8–C9 is 1.448 Å as both atoms are substituted. These results indicate that the ferrocene skeleton is slightly distorted. There is no hydrogen bond existed in the structure. The DPFEB is packed to form three dimensional crystals under the effect of Van der Waals force. Due to the numerous aromatic rings existed in the structure, the crystal is further stabilized by π–π interactions.

Heat capacity of DPFEB

The reproducibility and accuracy of the TMDSC (Q1000) were assessed by measuring the heat capacity of standard sapphire (α-Al_2O_3). The assessments were reported in our previous studies [23, 24]. The results indicated that the

Table 3 The data of three reduplicate DSC experiments for DPFEB

T/K	C_p (exp)/J K^{-1} g^{-1}				Standard deviation	T/K	C_p (exp)/J K^{-1} g^{-1}				Standard deviation
	1	2	3	Average			1	2	3	Average	
200	1.5264	1.5452	1.2902	1.4539	0.142	365	2.2989	2.3463	2.2064	2.2839	0.071
205	1.5312	1.5474	1.324	1.4675	0.125	370	2.3233	2.3711	2.2305	2.3083	0.072
210	1.5521	1.5681	1.3657	1.4953	0.112	375	2.3376	2.3884	2.2481	2.3247	0.071
215	1.5744	1.5916	1.4064	1.5241	0.102	380	2.3591	2.4117	2.2716	2.3475	0.071
220	1.5957	1.6156	1.4401	1.5505	0.096	385	2.3788	2.4356	2.294	2.3694	0.071
225	1.6164	1.6394	1.4706	1.5755	0.092	390	2.4013	2.4593	2.3181	2.3929	0.071
230	1.64	1.6679	1.4997	1.6025	0.09	395	2.4212	2.4866	2.3421	2.4166	0.072
235	1.6624	1.6971	1.528	1.6292	0.089	400	2.4417	2.5095	2.367	2.4394	0.071
240	1.6827	1.7249	1.5557	1.6544	0.088	405	2.4634	2.5319	2.391	2.4621	0.07
245	1.7053	1.7554	1.5829	1.6812	0.089	410	2.4816	2.5601	2.4155	2.4857	0.072
250	1.7294	1.7856	1.6131	1.7094	0.088	415	2.503	2.5816	2.4401	2.5082	0.071
255	1.7545	1.8076	1.6413	1.7345	0.085	420	2.5232	2.6075	2.4624	2.5311	0.073
260	1.7729	1.8249	1.6688	1.7555	0.079	425	2.5452	2.6337	2.4901	2.5563	0.072
265	1.7944	1.8451	1.6995	1.7797	0.074	430	2.5712	2.6646	2.5194	2.585	0.074
270	1.8227	1.8672	1.7266	1.8055	0.072	435	2.5998	2.697	2.5492	2.6153	0.075
275	1.8517	1.893	1.7569	1.8339	0.07	440	2.6293	2.7303	2.5844	2.648	0.075
280	1.8809	1.9214	1.7854	1.8626	0.07	445	2.6691	2.7769	2.6298	2.6919	0.076
285	1.9125	1.9492	1.8143	1.892	0.07	450	Phase transition region				
290	1.9403	1.9763	1.8414	1.9193	0.07	455					
295	1.9688	2.0024	1.8683	1.9465	0.07	460					
298.15	1.9867	2.0197	1.8855	1.964	0.07	465					
300	1.9948	2.0277	1.8954	1.9726	0.069	470					
305	2.0227	2.0554	1.9243	2.0008	0.068	475					
310	2.0478	2.0834	1.9528	2.028	0.067	480	3.0046	3.1336	2.9737	3.0373	0.085
315	2.0735	2.106	1.978	2.0525	0.067	485	3.0142	3.1431	2.9788	3.0453	0.086
320	2.0981	2.1332	2.0031	2.0782	0.067	490	3.0289	3.2036	2.99	3.0742	0.114
325	2.1234	2.1612	2.0275	2.104	0.069	495	3.0502	3.2043	3.0051	3.0865	0.104
330	2.1453	2.1861	2.0518	2.1277	0.069	500	3.0667	3.217	3.0248	3.1028	0.101
335	2.1697	2.2107	2.0751	2.1518	0.07	505	3.0887	3.2368	3.0362	3.1206	0.104
340	2.1929	2.2322	2.0974	2.1742	0.069	510	3.1088	3.2504	3.0529	3.1374	0.102
345	2.216	2.2566	2.121	2.1979	0.07	515	3.1272	3.2665	3.0675	3.1537	0.102
350	2.2355	2.2787	2.1424	2.2189	0.07	520	3.1481	3.2856	3.0831	3.1723	0.103
355	2.2574	2.301	2.1613	2.2399	0.071	525	3.1693	3.3104	3.1037	3.1945	0.106
360	2.279	2.3229	2.1835	2.2618	0.071	530	3.1909	3.331	3.1296	3.2171	0.103

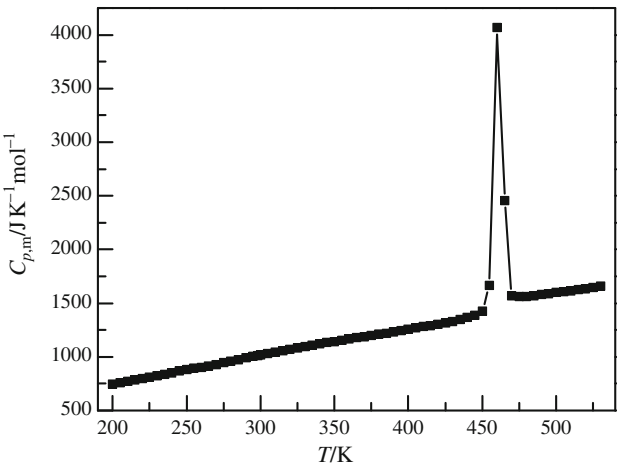

Fig. 2 The molar heat capacity of DPFEB as a function of temperature

testing system of TMDSC was steady and the measurement result was reliable.

The heat capacity data of DPFEB obtained through three duplicated experiments and the experimental standard deviation are given in Table 3. Experimental standard deviations below 0.14 are obtained and show reasonably good reproducibility in the temperature range of 200–530 K. The experimental molar heat capacity of DPFEB obtained based on the data listed in Table 3 is shown in Fig. 2. It can be seen that there is only one thermal anomaly existed in the temperature range of 450–475 K. The thermal anomaly is caused by the solid–liquid phase transition of DPFEB. In the temperature range of 200–445 K and 480–530 K, the heat capacity of DPFEB increases monotonically in a smooth and continuous manner, indicating that DPFEB is stable in the corresponding temperature range. It is known that molecules of a material in liquid are freer than in solid state. As a result, the C_p of liquid would be larger than that of solid. This phenomenon has been exhibited in our previous study [27–30] and Fig. 2 shows the phenomenon obviously.

The molar heat capacity of DPFEB is fitted to the following polynomial equations by means of nonlinear least square fitting through the OriginPro 8 software:

For the solid phase over the temperature range of 200–445 K:

$$C_{p,\mathrm{m}} = 1076.43 + 316.12X - 60.06X^2 - 33.71X^3 + 49.42X^4 + 36.94X^5, \quad (1)$$

where $X = (T - 322.5)/122.5$, and T is the experimental temperature, 322.5 is obtained from polynomial $(T_{\max} + T_{\min})/2$, and 122.5 is obtained from polynomial $(T_{\max} - T_{\min})/2$. $T_{\max}$ is the upper limit (445 K) of the above temperature region and $T_{\min}$ is the lower limit (200 K) of the above temperature region. The correlation coefficient of the fitting is $R^2 = 0.99993$.

For the liquid phase over the temperature of 480–530 K:

$$C_{p,\mathrm{m}} = 1608.35 + 39.43X - 1.93X^2 + 19.11X^3 + 4.92X^4 - 11.99X^5, \quad (2)$$

where $X = (T - 505)/25$, and T is the experimental temperature, 505 is obtained from polynomial $(T_{\max} + T_{\min})/2$, and 25 is obtained from polynomial $(T_{\max} - T_{\min})/2$. $T_{\max}$ is the upper limit (530 K) of the above temperature region and $T_{\min}$ is the lower limit (480 K) of the above temperature region. The correlation coefficient of the fitting is $R^2 = 0.99657$. The data of experimental and simulated molar heat capacities are listed in Table 4.

Thermodynamic functions of DPFEB

The phase transition molar enthalpy ΔH_{m} of DPFEB can be obtained by the integration of C_p–T curve from 450 to 480 K. The entropy ΔS_{m} of the phase transition of DPFEB can be derived according to the following equation:

$$\Delta S_{\mathrm{m}} = \Delta H_{\mathrm{m}}/T_{\mathrm{m}} \quad (3)$$

where T_{m} is the peak temperature of the curve. The values of the T_{m}, ΔH_{m}, and ΔS_{m} of the phase transition of DPFEB are determined to be 462.98 K, 35.76 kJ mol^{-1}, and 77.23 J mol^{-1} K^{-1}, respectively.

Enthalpy and entropy are important basic thermodynamic function of substances. Based on the polynomials of molar heat capacity and the thermodynamic relationships, the $[H_T - H_{298.15}]$ and $[S_T - S_{298.15}]$ of DPFEB are calculated over the experimental temperature range with an interval of 5 K relative to the temperature of 298.15 K. The thermodynamic relationships are as follows:

Before melting:

$$H_T - H_{298.15} = \int_{298.15}^{T} C_{p,\mathrm{m}}(s)\mathrm{d}T \quad (4)$$

$$S_T - S_{298.15} = \int_{298.15}^{T} \frac{C_{p,\mathrm{m}}(s)}{T}\mathrm{d}T. \quad (5)$$

After melting:

$$H_T - H_{298.15} = \int_{298.15}^{T_i} C_{p,\mathrm{m}}(s)\mathrm{d}T + \Delta_{\mathrm{fus}}H_{\mathrm{m}} + \int_{T_f}^{T} C_{p,\mathrm{m}}(l)\mathrm{d}T \quad (6)$$

Table 4 The experimental and simulated molar heat capacities of DPFEB

T/K	$C_{p,m}$ (exp)/J K^{-1} mol^{-1}	$C_{p,m}$ (fit)/J K^{-1} mol^{-1}	RD%	T/K	$C_{p,m}$ (exp)/J K^{-1} mol^{-1}	$C_{p,m}$ (fit)/J K^{-1} mol^{-1}	RD%
200	749.32	746.46	−0.38	365	1177.05	1178.37	0.11
205	756.33	759.54	0.42	370	1189.62	1189.46	−0.013
210	770.62	772.60	0.26	375	1198.09	1200.41	0.19
215	785.49	785.64	0.018	380	1209.82	1211.33	0.12
220	799.08	798.68	−0.050	385	1221.14	1222.24	0.090
225	811.95	811.81	−0.017	390	1233.23	1233.16	−0.0054
230	825.90	825.01	−0.11	395	1245.46	1244.23	−0.099
235	839.61	838.29	−0.16	400	1257.20	1255.51	−0.13
240	852.65	851.63	−0.12	405	1268.90	1267.08	−0.14
245	866.43	865.11	−0.15	410	1281.07	1279.05	−0.16
250	880.97	878.69	−0.26	415	1292.67	1291.50	−0.090
255	893.89	892.30	−0.18	420	1304.43	1304.62	0.015
260	904.75	906.05	0.14	425	1317.46	1318.53	0.081
265	917.20	919.87	0.29	430	1332.25	1333.32	0.080
270	930.49	933.69	0.34	435	1347.87	1349.25	0.10
275	945.12	947.57	0.26	440	1364.71	1366.46	0.13
280	959.92	961.46	0.16	445	1387.34	1385.13	−0.16
285	975.07	975.34	0.028	450	Phase transition region		
290	989.16	989.14	−0.0024	455			
295	1003.17	1002.92	−0.026	460			
298.15	1012.17	1011.55	−0.061	465			
300	1016.64	1016.60	−0.0040	470			
305	1031.16	1030.18	−0.096	475			
310	1045.17	1043.57	−0.15	480	1565.33	1564.79	−0.035
315	1057.80	1056.86	−0.088	485	1569.48	1571.73	0.14
320	1071.02	1069.97	−0.098	490	1584.34	1581.43	−0.18
325	1084.35	1082.84	−0.14	495	1590.71	1591.28	0.036
330	1096.57	1095.55	−0.094	500	1599.11	1600.23	0.070
335	1108.98	1108.04	−0.084	505	1608.24	1608.36	0.0073
340	1120.50	1120.31	−0.017	510	1616.91	1616.33	−0.036
345	1132.72	1132.31	−0.036	515	1625.35	1625.02	−0.020
350	1143.54	1144.14	0.053	520	1634.89	1635.15	0.016
355	1154.38	1155.75	0.12	525	1646.34	1646.53	0.012
360	1165.68	1167.13	0.12	530	1658.01	1657.90	−0.0068

$$S_T - S_{298.15} = \int_{298.15}^{T_i} \frac{C_{p,\mathrm{m}}(s)}{T}\mathrm{d}T + \Delta_{\mathrm{fus}}S_{\mathrm{m}} + \int_{T_f}^{T} \frac{C_{p,\mathrm{m}}(l)}{T}\mathrm{d}T, \tag{7}$$

where T_i is the temperature at which the melting started and T_f is the temperature at which the melting ended. The calculated thermodynamic functions $[H_T - H_{298.15}]$ and $[S_T - S_{298.15}]$ of DPFEB are shown in Table 5.

TG analysis

The TG and DTG curves of DPFEB are shown in Fig. 3. It can be seen that DPFEB started to pyrolysis at the temperature of 530 K, followed by a three step thermal decomposition. The first and the second steps of weight loss take place over the temperature range of 530–880 K. It seems that these two steps are partially overlapped, with a total weight loss of about 68.4%. The third step of thermal decomposition take place over the temperature range of

Table 5 Calculated thermodynamic function data of DPFEB

T/K	$H_T - H_{198.15}$/ kJ mol^{-1}	$S_T - S_{298.15}$/ J K^{-1} mol^{-1}	T/K	$H_T - H_{198.15}$/ kJ mol^{-1}	$S_T - S_{298.15}$/ J K^{-1} mol^{-1}	T/K	$H_T - H_{198.15}$/ kJ mol^{-1}	$S_T - S_{298.15}$/ J K^{-1} mol^{-1}
200	−86.1	−346.75	310	12.17	40.03	425	148.14	410.86
205	−82.34	−328.19	315	17.43	56.86	430	154.75	426.33
210	−78.51	−309.71	320	22.75	73.62	435	161.46	441.84
215	−74.61	−291.38	325	28.12	90.27	440	168.26	457.37
220	−70.66	−273.2	330	33.57	106.91	445	175.13	472.91
225	−66.63	−255.08	335	39.09	123.5	450	Phase transition region	
230	−62.53	−237.08	340	44.66	140.02	455		
235	−58.37	−219.18	345	50.28	156.43	460		
240	−54.16	−201.43	350	55.98	172.82	465		
245	−49.86	−183.72	355	61.73	189.15	470		
250	−45.5	−166.09	360	67.53	205.36	475		
255	−41.08	−148.6	365	73.4	221.55	480	210.89	550.14
260	−36.58	−131.13	370	79.32	237.67	485	218.72	566.39
265	−32.01	−113.72	375	85.28	253.67	490	226.59	582.56
270	−27.39	−96.43	380	91.32	269.66	495	234.52	598.66
275	−22.68	−79.16	385	97.41	285.59	500	242.49	614.7
280	−17.91	−61.95	390	103.54	301.39	505	250.54	630.67
285	−13.06	−44.79	395	109.73	317.18	510	258.61	646.55
290	−8.16	−27.75	400	115.99	332.92	515	266.68	662.36
295	−3.17	−10.7	405	122.3	348.59	520	274.85	678.11
298.15	0	0	410	128.67	364.23	525	283.05	693.81
300	1.88	6.28	415	135.08	379.77	530	291.32	709.47
305	7	23.21	420	141.57	395.33			

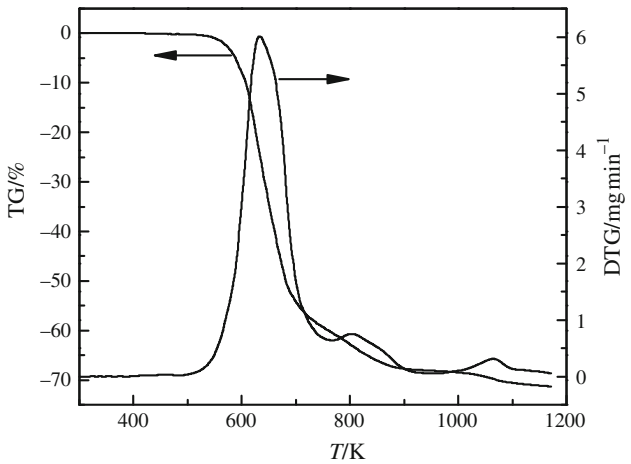

Fig. 3 TG and DTG curves of DPFEB in nitrogen

1000–1120 K with the weight loss of about 2.9%. When it was heated in nitrogen atmosphere, DPFEB experienced a process of carbonization and incineration, so that the residue should be composed of carbon and iron phosphine [31].

Conclusions

In general, a new potential enantioselective catalyst derived from ferrocene, DPFEB, was prepared through a two step procedure from (*R*)-Ugi's amine. The absolute structure was characterized by means of single crystal X-ray diffraction. The molar heat capacity of DPFEB was measured by means of TMDSC over the temperature range of 200–530 K. There was a solid–liquid phase transition occurred from 450 to 475 K with the ΔH_m of 35.76 kJ mol^{-1}. The thermodynamic functions of $[H_T - H_{298.15}]$ and $[S_T - S_{298.15}]$ were calculated based on the heat capacity data. Further more, thermogravimetry experiment revealed that DPFEB exhibited a three steps thermal decomposition process with the final residual of 28.7% in nitrogen atmosphere.

Acknowledgements This study was financially supported by the National Natural Science Foundation of China (21003014, 21075011 and 20775010), Hunan Provincial Science and Technology Project (2010FJ3167, 2007NK3123), Hunan Provincial Natural Science Foundation of China (09JJ3016, 09JJ3035), Program for New Century Excellent Talents in University (NCET-10-0138, Ministry of Education of the People's Republic of China), Hunan Provincial Key Laboratory of Materials Protection for Electric Power and Transportation

(Changsha University of Science & Technology) (2010CL07), and Changsha University of Science & Technology.

References

1. Padeste C, Steiger B, Grubelnik A, Tiefenauer L. Molecular assembly of redox-conductive ferrocene–streptavidin conjugates—towards bio-electrochemical devices. Biosens Bioelectron. 2004;20:545–52.
2. Morad MS, Sarhan AAO. Application of some ferrocene derivatives in the field of corrosion inhibition. Corros Sci. 2008;50:744–53.
3. Liu Y, Dong SJ. A biofuel cell with enhanced power output by grape juice. Electrochem Commun. 2007;9:1423–7.
4. Hudson RDA. Ferrocene polymers: current architectures, syntheses and utility. J Organomet Chem. 2001;637:47–69.
5. Wright ME, Laub J, Stafford PR, Norris WP. Synthesis of new ferrocene containing diamines and their use in epoxy resins. J Organomet Chem. 2001;637–639:837–40.
6. Sarhan AAO. Synthesis and applications of tetrathiafulvalenes and ferrocene-tetrathiafulvalenes and related compounds. Tetrahedron. 2005;61:3889–932.
7. Atkinson RCJ, Gibson VC, Long NJ. The syntheses and catalytic applications of unsymmetrical ferrocene ligands. Chem Soc Rev. 2004;33:313–28.
8. Blaser HU, Pugin B, Spindler F. Progress in enantioselective catalysis assessed from an industrial point of view. J Mol Catal A Chem. 2005;231:1–20.
9. Chapelon AS, Moraléda D, Rodriguez R, Ollivier C, Santelli M. Enantioselective synthesis of steroids. Tetrahedron. 2007;63:11511–616.
10. Ohno A, Yamane M, Hayashi T, Oguni N, Hayashi M. Preparation and use of chiral ferrocenylphosphines containing new alkyl substituents on the ferrocenylmethyl position. Tetrahedron Asymmetry. 1995;6:2495–502.
11. Wang DY, Hu XP, Hou CJ, Deng J, Yu SB, Duan ZC, Huang JD, Zheng Z. Enantioselective Rh-catalyzed hydrogenation of 3-aryl-2-phosphonomethylpropenoates by a new class of chiral ferrocenyl diphosphine ligands. Org Lett. 2009;11:3226–9.
12. Richards CJ, Locke AJ. Recent advances in the generation of non-racemic ferrocene derivatives and their application to asymmetric synthesis. Tetrahedron Asymmetry. 1998;9:2377–407.
13. Zeng W, Zhou YG. Bifunctional AgOAc catalyzed asymmetric [3 + 2] cycloaddition of azomethine ylides. Org Lett. 2005;7:5055–8.
14. Domracheva LG, Karyakin NV, Sheiman MS, Kamelova GV, Larina VN, Suvorova ON, Domrachev GA. Thermodynamics and molecular dynamics of some ferrocene derivatives. Russ Chem Bull. 1999;48:1647–55.
15. Wunderlich B, Jin Y, Boller A. Mathematical-description of differential scanning calorimetry based on periodic temperature modulation. Thermochim Acta. 1994;238:277–93.
16. Wunderlich B. The contributions of MDSC to the understanding of the thermodynamics of polymers. J Therm Anal Calorim. 2006;85:179–87.
17. Divi S, Chellappa R, Chandra D. Heat capacity measurement of organic thermal energy storage materials. J Chem Thermodyn. 2006;38:1312–26.
18. Heidenreich S, Langner T, Rohm H. Heat capacity of cheese. J Therm Anal Calorim. 2007;89:815–9.
19. Chau J, Garlicka I, Wolf C, Teh J. Modulated DSC as a tool for polyethylene structure characterization. J Therm Anal Calorim. 2007;90:713–9.
20. Qiu SJ, Chu HL, Zhang J, Qi YN, Sun LX, Xu F. Heat capacities and thermodynamic properties of CoPc and CoTMPP. J Therm Anal Calorim. 2008;91:841–8.
21. Archer DG. Thermodynamic properties of synthetic sapphire (α-Al_2O_3), standard reference material 720 and the effect of temperature-scale differences on thermodynamic properties. J Phys Chem Ref Data. 1993;22:1441–53.
22. Ginnings DC, Furukawa GT. Heat capacity standards for the range 14 to 1200°K. J Am Chem Soc. 1953;75:522–7.
23. Gokel GW, Ugi IK. Preparation and resolution of *N*, *N*-dimethyl-*o*-ferrocenylethylamine. An advanced organic experiment. J Chem Edu. 1972;49:294–6.
24. Hayashi T, Mise T, Fukushima M, Kagotani M, Nagashima N, Hamada Y, Matsumoto A, Kawakami S, Konishi M, Yamamoto K, Kumada M. Asymmetric synthesis catalyzed by chiral ferrocenylphosphine–transition metal complexes. I. Preparation of chiral ferrocenylphosphines. Bull Chem Soc Jpn. 1980;53:1138–51.
25. Cheung HY, Yu WY, Lam FL, Au-Yeung TTL, Zhou ZY, Chan TH, Chan ASC. Enantioselective Pd-catalyzed allylic alkylation of indoles by a new class of chiral ferrocenyl P/S ligands. Org Lett. 2007;9:4295–8.
26. Sheldrick GM. SHELX97, Program for crystal structure refinement. Germany: Göttigen University; 1997.
27. Zhang ZH, Cui T, Zhang JL, Xiong H, Li GP, Sun LX, Xu F, Cao Z, Li F, Zhao JJ. Thermodynamic investigation of room temperature ionic liquid. The heat capacity and thermodynamic functions of $BMIPF_6$. J Therm Anal Calorim. 2010;101:1143–8.
28. Tong B, Yu Y, Tan ZC, Meng CG, Cui LJ, Xiao G, Liu RB. Thermodynamic investigation of several natural polyols (IV): heat capacities and thermodynamic properties of adonitol. Thermochim Acta. 2010;499:117–22.
29. Xue B, Li XF, Wang JY, Yu SJ, Tan ZC, Sun LX. Heat capacities and thermodynamic properties of trans-(R)-3-(2, 2-dichloroethenyl)-2, 2-dimethylcyclopropanecarboxylic acid. J Therm Anal Calorim. 2008;94:529–34.
30. Wang SX, Tan ZC, Li YS, Li Y, Shi Q, Tong B. Heat capacity and thermodynamic properties of benzyl disulfide ($C_{14}H_{14}S_2$). Thermochim Acta. 2007;463:21–5.
31. de Castro VD, de Lima GM, Porto AO, Siebald HGL, de Souza Filho JD, Ardisson JD, Ayala JD, Bombieri G. Synthesis, structural characterisation and thermal decomposition of [{Pt(dppf)(2-SPy)}{BF4}](dppf = 1,1′-bisdiphenylphosfinoferrocene and 2-Spy = 2-mercaptopyridine)—a source for a Fe–Pt containing alloy. Polyhedron. 2004;23:63–9.